ACS OMEGA

Open Access

http://pubs.acs.org/journal/acsodf

Article

Dissolution Behavior of Polycyclic Aromatic Hydrocarbons in Heavy Oil in the Presence of Supercritical Cyclohexane

Xiangbo Zhao, Litao Wang, Shuai Liu, Xuan Luo, Mengran Zhang, Feng Fu, Xiaoming Gao, and Ting Yan*

Cite This: *ACS Omega* 2024, 9, 252−263

Read Online

ACCESS | Metrics & More | Article Recommendations | Supporting Information

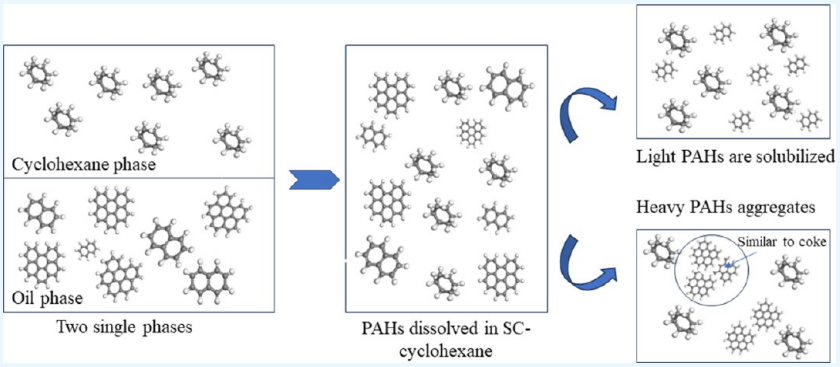

ABSTRACT: Supercritical cyclohexane (SC-cyclohexane) shows significant advantages in mild operating conditions and the modulation of product distribution. To gain insights into the upgrading process of heavy oil in SC-cyclohexane, the dissolution process of polycyclic aromatic hydrocarbons (PAHs) contained in heavy oil was simulated based on molecular dynamics with the use of naphthalene, benzopyrene, and mixtures of naphthalene and benzopyrene as the model compounds. As indicated by the radial distribution function results, in SC-cyclohexane exhibiting low density, cyclohexane formed a solvent shell around PAHs such that the local concentration was reduced and the aggregation of PAHs was inhibited. The results of the solvation free energy suggested that van der Waals forces between PAHs and cyclohexane were mainly dominant. As revealed by the dissolution process of the model compounds in SC-cyclohexane, a low density and a suitable temperature contributed to the solubilization of PAHs. An appropriate temperature and a low density can be selected for the upgrading reaction to limit coke formation.

1. INTRODUCTION

Despite the rapid advance of new energy sources, fossil resources still take on a critical significance to the development of human society. However, the content of light crude oil after long-term overexploitation and consumption cannot conform to the rapid development of society. Heavy oil and extra-heavy oil reserves have accounted for over 50% of the existing oil reserves worldwide.[1] The conventional hydrogenation process and the carbon rejection process have numerous limitations in heavy oil processing due to the characteristics of high viscosity and high content of heteroatoms.[2−5] The carbon rejection process will generate considerable coke such that a waste of resources is caused. Heteroatoms (e.g., S and N) in heavy oil deactivate the catalyst in the hydrogenation process. Supercritical fluids (SCFs) technology refers to a novel process that can reform heavy oil without the use of catalysts and inhibiting coke production.[6] SCFs have been extensively employed in upgrading and visbreaking of heavy oil.[7−11] Heavy oils can dissolve into supercritical water (SCW) with a low dielectric constant and good diffusion properties. Under the effect of the potential hydrogen supply capacity, the upgrading and viscosity reduction of heavy oil in SCF is primarily concentrated in SCW.[12−14]

Existing research has suggested that by changing SCFs and their thermodynamic parameters, a variety of phase structures (e.g., two-phase, three-phase, and pseudo-phase) can be obtained. Different phase structures and the corresponding diffusion environment are considered to be critical in the noncatalytic pyrolysis of heavy oils in SCF.[15−17] However, the mixed systems of water and hydrocarbons exhibit complex phase behavior. The focus of relevant research has been the detection and prediction of their complex phase behavior.[18] Existing research has investigated, the phase behavior of water with many low-molecular-weight hydrocarbons.[19] Heavy

Received: June 10, 2023
Revised: November 20, 2023
Accepted: November 22, 2023
Published: December 26, 2023

hydrocarbon mixtures have been rarely investigated since both the opacity and emulsification of the mixture may interfere with phase boundary measurements. Moreover, the pyrolysis process of hydrocarbons at high temperatures and under high pressure is difficult in sampling such that it is challenging to measure the phase behavior of such mixtures. Molecular dynamics (MD) simulation is capable of studying complex systems at the supercritical state.[20,21] Zhou et al.[22] explored the structure and diffusion properties of SCW through MD simulations. The calculations confirmed that the average number of hydrogen bonds and the cluster size decline with the increase of the temperature and with the decrease of the density. Xin et al.[23] studied the solvation effect of asphaltenes in SCF through MD simulation. The repulsive van der Waals interaction significantly affects the interaction between asphaltene molecules and water molecules. Qu et al.[3] simulated the dissolution of polycyclic aromatic hydrocarbons (PAHs) with different ring numbers in sub-CW/SCW. During the dissolution of oil droplets comprising a mixture of PAHs, the light PAHs preferentially dissolve into the aqueous phase, and the heavy PAHs are concentrated in the oil droplets exhibiting smaller volumes. Novel SCF with good solubility for hydrocarbons has started to serve as solvents for heavy oil reforming due to SCW's thermodynamic lack of hydrogen supply capability and insufficient solubility, leading to heavy oil coking in large quantities. Liu et al.[24] studied the visbreaking of heavy oils in supercritical benzene (SC-C_6H_6). The viscosity of product oil was significantly reduced, and asphaltene formation was inhibited at low temperatures (i.e., as low as 340 °C). However, SC-C_6H_6 cannot supply hydrogen in the pyrolysis of heavy oils. Accordingly, a supercritical hydrocarbon exhibiting a hydrogen supply capability serves as a promising solvent for heavy oil pyrolysis. Ding et al.[25] confirmed that supercritical cyclohexane (SC-cyclohexane, T_c = 280.4 °C, P_c = 4.05 MPa) plays a certain role in the reaction through H supply. SC-cyclohexane, a hydrogen donor and reaction solvent, is more suitable than SCW and SC-C_6H_6 in reducing the viscosity of heavy oil, increasing the H/C atomic ratio, and inhibiting coke formation. However, the dissolution behavior of heavy oil in SC-cyclohexane has been rarely investigated to explain the pyrolysis of heavy oil in depth.

In this study, the dissolution behavior of PAHs in SC-cyclohexane was investigated by using the MD method, and the effect of dissolution on the pyrolysis of PAHs was clarified. First, the dissolution behaviors of light PAH, heavy PAH, and PAH mixtures in SC-cyclohexane were investigated using the MD simulation method, and the effects of the scale of PAHs and the composition of PAH mixtures on the dissolution process were determined. The interaction of PAHs with the SC-cyclohexane environment was characterized in accordance with the analysis result of the short-range solvent structure and solvation free energy of PAHs in SC-cyclohexane. Subsequently, the interactions between PAHs were determined by calculating the cohesion energy density among PAHs. This study can provide theoretical guidance for the screening of the solvent in the reforming of heavy oil in SCF and the determination of the operating range.

2. METHODOLOGY

2.1. Model Selection. Only PAHs without heteroatoms and alkyl substituents were considered in this study to improve the calculation efficiency since the structure of PAHs contained in heavy oil is very complex. Naphthalene (NAP) served as the light PAH, and benzo[ghi]perylene (BghiP) was selected as the heavy PAH as shown in Supporting Figure 1. Supporting Table 1 lists the details of these PAHs.

2.2. Simulation Procedures. All of the optimizations of molecule structures employed for simulation and MD simulation were performed using Materials Studio 2019 software. Moreover, all of the density functional theory (DFT) calculations were performed with the Gaussian 09 software in accordance with the B3LYP/6-311G (2d,p) level of theory.[26]

2.3. Simulation Details. First, the solvent environment was simulated based on molecular dynamics. A periodic cubic solvent box was built at a side length of 80 Å. The solvent box was filled with a fixed number of cyclohexane molecules (100−300), which was dependent on the cyclohexane density. The COMPASS force field employed in the simulation has been proven to be reliable and accurate. The calculations were conducted in accordance with the Forcite module of the Materials Studio 2019 software. The temperature was regulated with an NHL thermostat (634−674 K) throughout the simulation. The electrostatic method and the van der Waals summation method were set on the van der Waals bases and atomic methods, respectively. During the calculation of the radial distribution function (RDF) and the solvation free energy G_{sol}, only one PAH molecule was placed in the solvent box that was randomly surrounded by cyclohexane molecules. The RDF of gPAHs-H(r) between the PAH molecule and the hydrogen atoms in cyclohexane was determined based on the recorded trajectory file after 500 ps simulation such that the calculation was ensured to be in equilibrium.

Using the coupling parameter method proposed by Kirkwood,[27] the G_{sol} of PAHs in SC-cyclohexane is expressed as

$$G_{sol} = G_{id} + G_{elec} + G_{vdw} \quad (1)$$

where G_{id} and G_{vdw} denote the free energy of removing charges from PAH molecules in a vacuum and the free energy of adding neutralized PAH molecules into the solvent, respectively, and G_{elec} represents the free energy of adding charges on PAH molecules, as well as interacting with the solvent.

The cohesive energy density (CED) of PAHs indicates the strength of intermolecular interactions of PAHs, and it is the average energy required to separate all molecules to infinity. The value of CED is written as

$$CED = \Delta H_{vap} - RT \quad (2)$$

where ΔH_{vap} denotes the enthalpy of evaporation of PAHs. R and T represent the gas constants and temperature, respectively.

A standard metric for the size of polymers or other macromolecules in solution represents the radius of gyration (R_g),[28] defined as

$$R_g^2 = \frac{1}{N}\sum_{k=1}^{N}(r_k - r_{cm})^2 \quad (3)$$

where r_k denotes the position vector of atom k and r_{cm} expresses the position vector of the center of mass of the cluster.

Mean-square deviation (MSD) analysis refers to a technique that determines the mode of displacement of the polymer

https://doi.org/10.1021/acsomega.3c04101
ACS Omega 2024, 9, 252−263

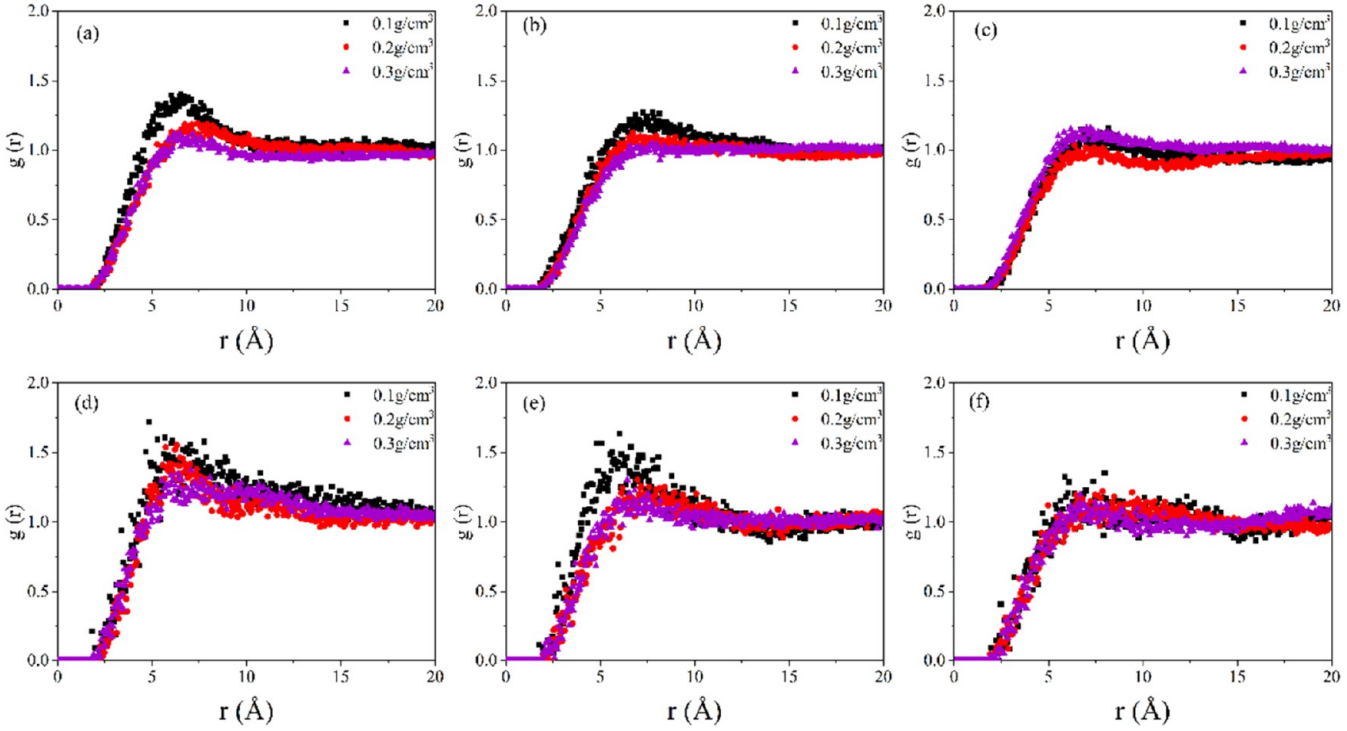

Figure 1. $g_{\text{nap-H}}(r)$ and $g_{\text{BghiP-H}}(r)$ at different densities: (top) $g_{\text{nap-H}}(r)$: (a−c) 634−674 K; (bottom) $g_{\text{BghiP-H}}(r)$: (d−f) 634−674 K.

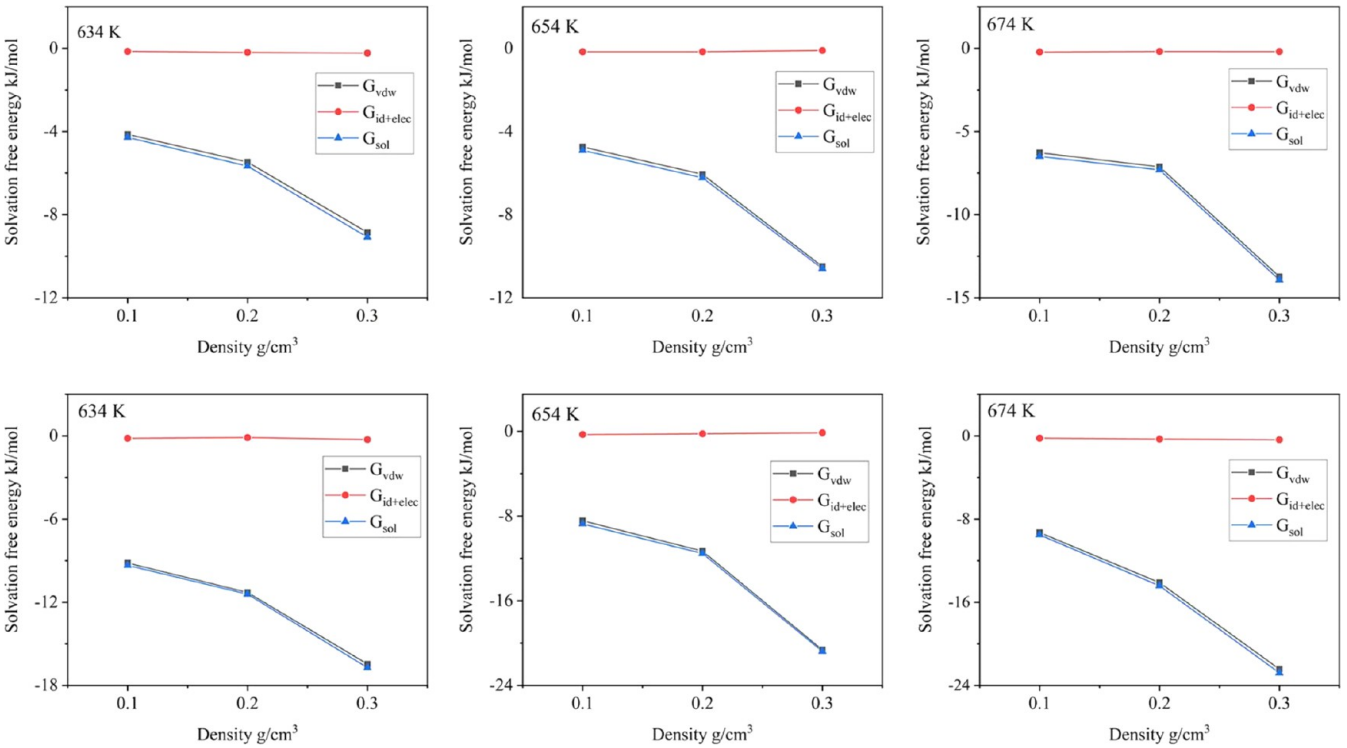

Figure 2. G_{sol}'s of NAP and BghiP in SC-cyclohexane at various densities and temperatures: (top) NAP, (bottom) BghiP.

followed over time. Notably, it is conducive to determining whether the polymer is freely diffusing, transported, or bound.

$$\text{MSD}\ (\Delta t) = \langle [r(t + \Delta t) - r(t)]^2 \rangle \tag{4}$$

where $r(t)$ denotes the position at time t and $r(t + \Delta t)$ represents the position at an interval Δt later. The squared displacement of the particle during that interval is expressed as $r(t + \Delta t) - r(t)^2$.

An oil droplet comprising multiple PAH molecules with a radius of 15 Å was built to simulate the dissolution behavior of PAHs in SC-cyclohexane. The droplet was placed in the center of the previously built solvent box after structural optimization and an annealing operation. Subsequently, MD simulations

https://doi.org/10.1021/acsomega.3c04101
ACS Omega 2024, 9, 252−263

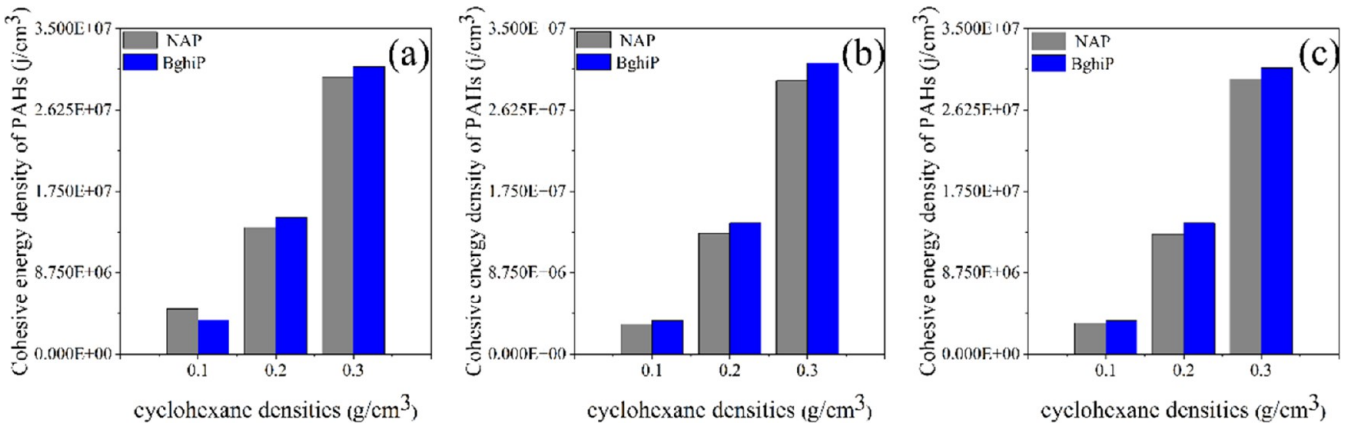

Figure 3. Cohesive energy density of PAHs under different densities and temperatures: (a−c) 634−674 K.

based on the NVT system were performed for 500 ps to ensure the kinetic equilibrium. The dissolution behavior of PAHs droplets in SC-cyclohexane was determined using solvent box snapshots under different simulation conditions and different simulation times.

3. RESULT AND DISCUSSION

3.1.1. Radial Distribution Function. The miscibility of PAHs with SC-cyclohexane is dependent on two factors (i.e., solute−solvent interactions and solute−solute interactions). The proximity solvent structure and solvation free energy of PAHs in SC-cyclohexane indicate solute−solvent interactions in system.[3] The radial distribution functions (RDF) of $g_{\text{BghiP-H}}(r)$ and $g_{\text{NAP-H}}(r)$ in cyclohexane with densities of 0.10−0.30 g/cm^3 at 634, 654, and 674 K were determined to account for the solvent structure of PAHs in SC-cyclohexane. The results are shown in Figure 1.

The RDFs of $g_{\text{BghiP-H}}(r)$ at 0.1−0.3 g/cm^3 displayed a similar trend at 634 K. The value of $g_{\text{BghiP-H}}(r)$ remained at 0 within the radius of the BghiP molecule. The value of $g_{\text{BghiP-H}}(r)$ began to increase gradually as the radius exceeded 2.5 Å, reaching a maximum at 7.5 Å. Subsequently, the value of $g_{\text{BghiP-H}}(r)$ started to decrease and approached 1 at a radius of nearly 10 Å to be maintained. Different characteristic peaks of $g_{\text{BghiP-H}}(r)$ were observed at different temperatures. With the increase in the density, the corresponding peak height was decreased, suggesting that the SC-cyclohexane with a lower density was subjected to a stronger interaction with heavy PAHs. Moreover, the interaction between Bghip and cyclohexane was reduced with an increase in temperature. For NAP, the trends of its RDFs were the same as those of BghiP. In addition, the interaction between NAP and SC-cyclohexane was decreased with the increase of the temperature and the density. The interaction between NAP and cyclohexane was probably weaker than that between Bghip and cyclohexane, probably. Because NAP exhibits weaker aromaticity than BghiP. As revealed by the conclusion of the previous reports, a solvation shell was formed by cyclohexane molecules around the PAHs.[29,30] The solvent shell is capable of spatially hindering the agglomeration of PAH molecules.

3.1.2. Solvation Free Energy. The Gibbs solvation free energy refers to another parameter that indicates the solute−solvent interaction in the system. The sum of G_{id} and G_{elec} was adopted to characterize the contribution of polar components to G_{sol}. G_{vdw} was adopted to express the contribution of nonpolar components to G_{sol}. The G_{sol}'s of NAP and BghiP in SC-cyclohexane were determined under different conditions, as shown in Figure 2. In the presence of SC-cyclohexane at three densities, the $G_{\text{id+elec}}$ of the PAH molecule maintained negligible values. The G_{vdw}'s of PAH became negative and several orders of magnitude larger than $G_{\text{id+elec}}$, suggesting that the van der Waals effect can take on dominant significance in the values and properties of G_{sol} of PAH molecules in the presence of SC-cyclohexane. PAH molecules and cyclohexane molecules were attracted to each other. With the increase of the density, the G_{sol}'s of both NAP and BghiP were increased monotonically, suggesting that higher energy is required for the solvation of PAHs in SC-cyclohexane with high densities. Furthermore, the increase in the temperature led to an increase of the values of G_{sol}'s of NAP and BghiP. The comparison of the G_{sol}'s of NAP and BghiP with the different numbers of aromatic rings suggested that BghiP can be more difficult to solubilize in SC-cyclohexane.

3.1.3. Cohesive Energy Density. The cohesive energy density (CED) is capable of describing the interactions between PAHs. In this study, the CED of NAP and BghiP in SC-cyclohexane environment was determined at the corresponding temperatures and pressures, as shown in Figure 3.

In the SC-cyclohexane environment, the higher CED of PAHs can indicate a stronger interaction between PAHs.[3] As depicted in Figure 3, the CED between PAHs at low densities was significantly smaller than that at high densities. The reason for the above result is that at low densities, cyclohexane molecules can form a solvent shell around the PAHs, as indicated by the result of RDFs. The solvent shell can hinder the $\pi-\pi$ mutual attraction between PAHs. Thus, the cyclohexane environment at a low density can be conducive to weakening the mutual attraction between PAHs and inhibiting the polymerization reaction during the pyrolysis of PAHs.

The temperature exerted a weak effect on the CED of PAHs in SC-cyclohexane. As depicted in Figure 3, the CED of PAHs did not change significantly with the increase in temperature. Although an increase in the temperature can facilitate molecular thermal motion, inhibition of the attraction between PAHs by the solvent shell formed by cyclohexane can become dominant. The CED of BghiP was slightly greater than the CED of NAP since BghiP exhibits greater aromaticity than NAP.

3.1.4. Mean-Square Deviation (MSD) Analysis. MSD was employed to analyze the structural changes of PAH molecules at different operating parameters.[31] The structural changes of

https://doi.org/10.1021/acsomega.3c04101
ACS Omega 2024, 9, 252−263

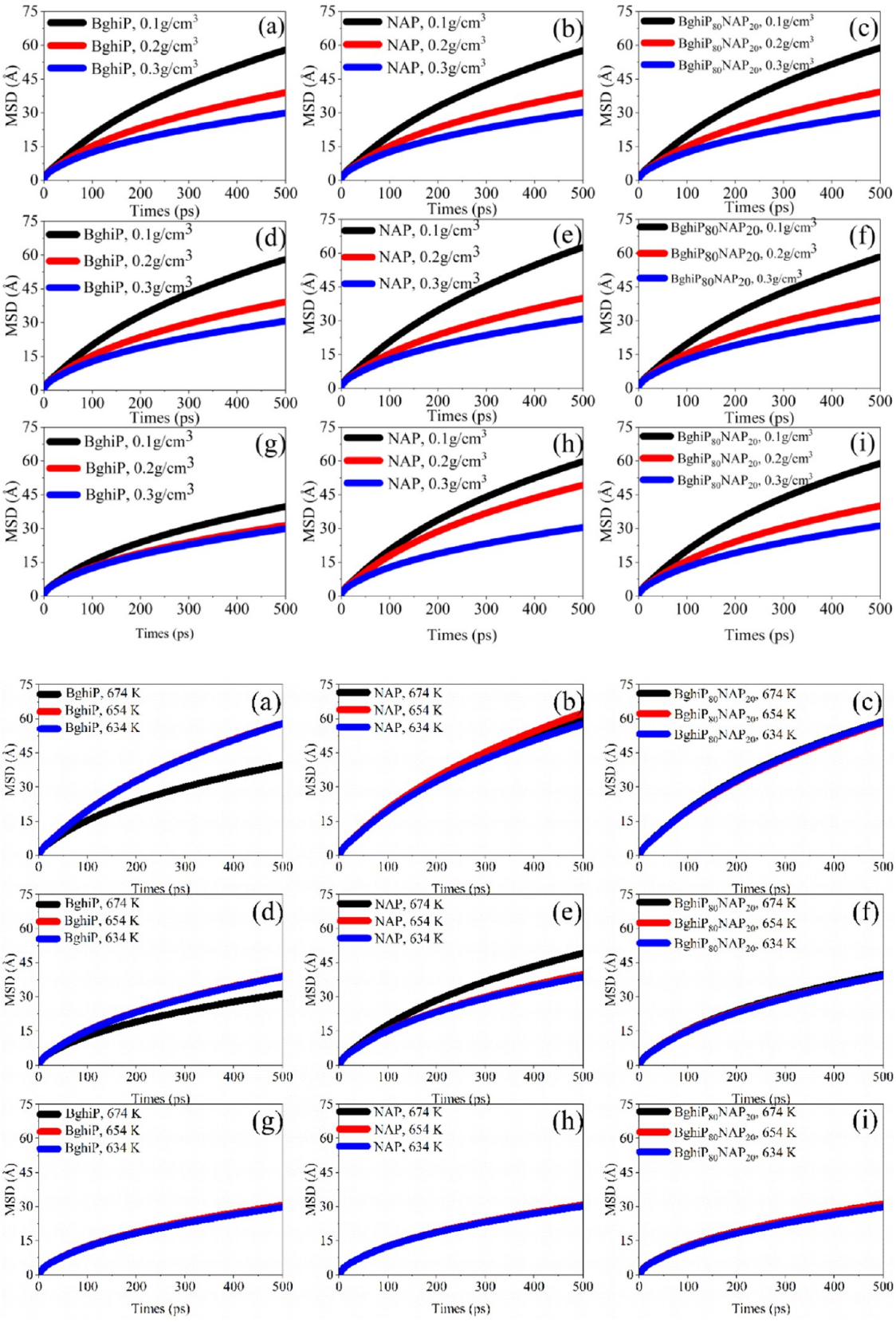

Figure 4. MSD of SC-cyclohexane the simulation trajectories in different temperatures and different densities: (top) (a−c) 634 K, (d−f) 654 K, (g−i) 674 K; (bottom) (a−c) 0.1 g/cm^3, (d−f) 0.2 g/cm^3, (g−i) 0.3 g/cm^3.

oil drops comprising NAP molecules, oil drops comprising BghiP molecules, and oil drops comprising NAP and BghiP mixtures in solvents of different densities and temperatures were determined by removing the first 50 ns of the equilibrium phase through the MSD analysis. As depicted in Figure 4, the lowest MSD values were observed for the three samples in 0.3

https://doi.org/10.1021/acsomega.3c04101
ACS Omega 2024, 9, 252−263

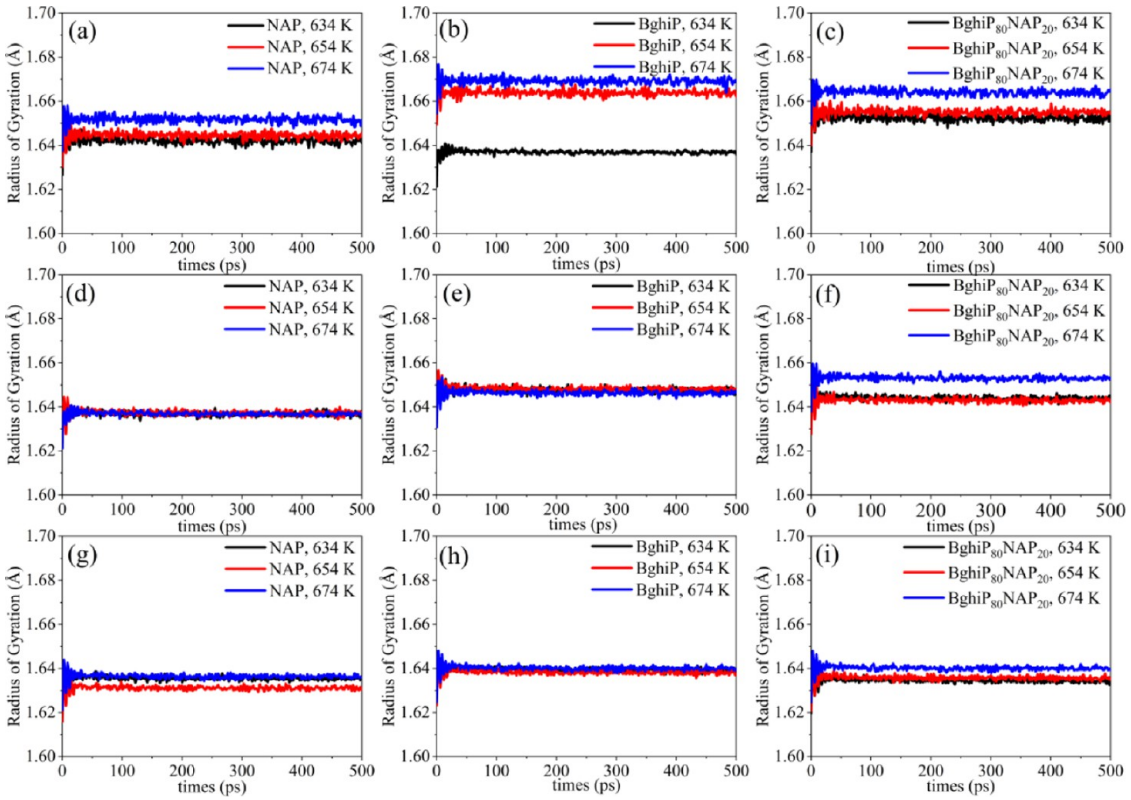

Figure 5. R_g of SC-cyclohexane of the simulation trajectories in different densities: (a–c) 0.1 g/cm^3, (d–f) 0.2 g/cm^3, (g–i) 0.3 g/cm^3.

g/cm^3 SC-cyclohexane, suggesting that the oil droplet structure of the three samples was more intact in SC-cyclohexane at 0.3 g/cm^3. The solubility of PAHs was the lowest in cyclohexane at 0.3 g/cm^3, consistent with the analytical results of RDF and G_{sol}.

As depicted in Figure 4, the effect of temperature on the MSD was decreased with the increase of the solvent density. In 0.1 g/cm^3 cyclohexane, the MSD of Bghip was decreased with the increase of the temperature. The reason for the above result is that an increase in the temperature can facilitate the polymerization of PAHs such that the stability of the oil droplet structure can be maintained (BghiP undergoes almost no structural changes due to dissociation). Although the solubility of BghiP gradually decreased with the rise of the solvent density, their structure remained relatively intact. As a result, the effect of temperature on the solubility of BghiP became insignificant. Since the aromaticity of NAP is weaker than that of BghiP, the promotion of NAP agglomeration by increasing temperature becomes weaker than the promotion of NAP molecule diffusion. The increase of temperature can facilitate the dissolution of NAP oil droplets in SC-cyclohexane. However, since the density of cyclohexane takes on a dominant significance to the dissolution process, the promotion effect of increasing temperature on the dissolution of NAP oil droplets was gradually weakened with the increase in density.

In general, the impact of the temperature on the three substances is not considerably different at high densities. However, at low densities, the temperature does not significantly affect the MSD for all three substances due to the limited aromaticity of NAP and its weaker self-interactions. On the other hand, for BghiP, the higher temperature of 674 K accelerates the thermal motion of the molecules, causing them to cluster together. As a consequence, the MSD at higher temperatures is smaller than the MSD at lower temperatures.

3.1.5. Radius of Gyration (R_g) Analysis. R_g denotes the compactness of the structure during the simulation, which is similar to that of the MSD curves (Figure 5). Figure 5 presents the R_g's of NAP droplets, BghiP droplets, and PAHs mixed droplets at the same density in 0.1 g/cm^3 SC-cyclohexane, and the R_g at 674 K reached the lowest among the three types of PAHs droplets. The R_g's of the NAP and PAHs mixture were the highest at 634 K, and the R_g of BghiP was the highest at 654 K. The reason for the above result is that the increase in the temperature can facilitate molecular thermal motion and $\pi-\pi$ stacking. Because of the difference in molecular structure, the structural changes due to molecular thermal motion and $\pi-\pi$ stacking canceled each other for the NAP and PAHs mixtures at 654 and 674 K. The structural tightening due to $\pi-\pi$ stacking exceeded the structural loosening due to molecular thermal motion for BghiP with the rise of the temperature.

The R_g's of PAH molecules in the 0.2 and 0.3 g/cm^3 systems were lower than that in 0.1 g/cm^3 at 674 K, suggesting that PAH molecules exhibited a tight structure at the two densities. As indicated by R_g in 0.1 g/cm^3, PAH molecules changed from a tight structure to a more extended polymer structure in their systems, whereas similar results were observed at 654 as well as 634 K, further suggesting that the PAH structure can be more disordered in the 0.1 g/cm^3 system and can dissolve well in SC-cyclohexane.

In brief, the effect of density on the dissolution of PAHs was stronger than that of temperature. Thus, both R_g and MSD suggested that the solubility of PAHs and PAH mixtures can be efficiently increased at low densities and appropriate temperatures. Furthermore, representative snapshots of MD simu-

https://doi.org/10.1021/acsomega.3c04101
ACS Omega 2024, 9, 252−263

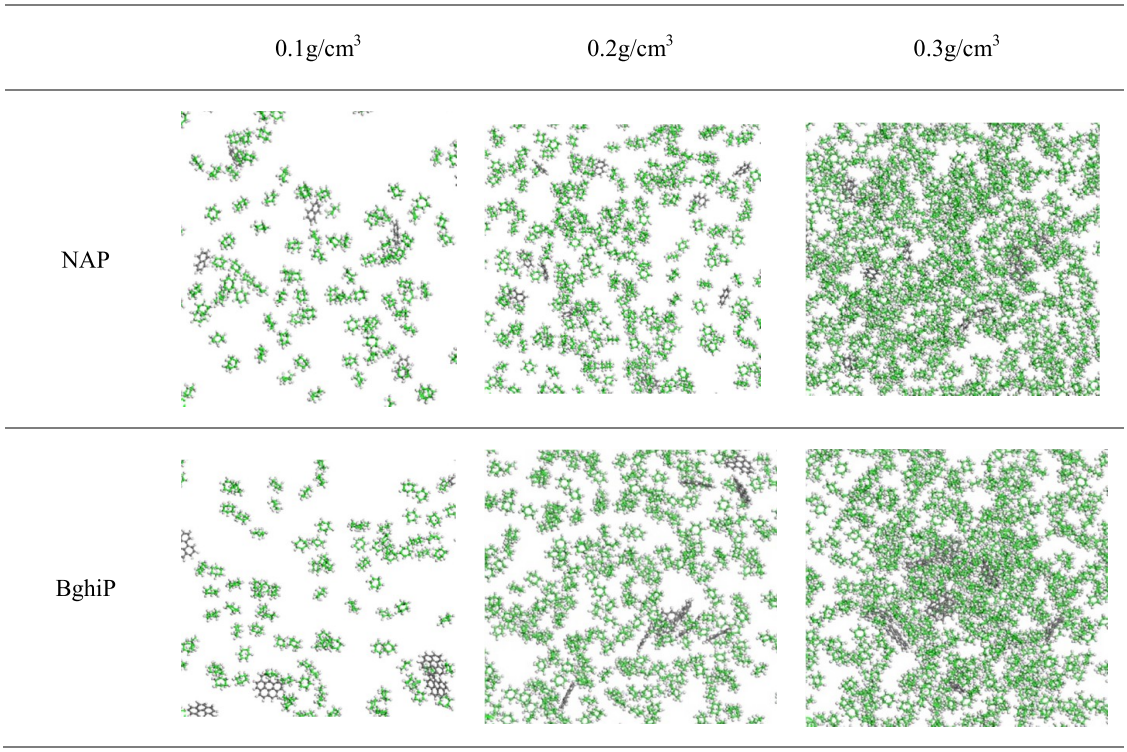

Figure 6. Dissolution of PAH droplets in SC-cyclohexane at different densities and temperature of 674 K.

lations were visualized to gain insight into the conformational changes in PAH molecules at different densities and temperatures, as presented in the following sections.

3.2. Dissolution of PAHs in SC-Cyclohexane. *3.2.1. Effect of Solvent Density.* The dissolution behaviors of PAH droplets containing NAPs and BghiPs in SC-cyclohexane with different densities were simulated through MD. The three densities of cyclohexane were set at 0.10, 0.20, and 0.30 g/cm^3. The pressures for different densities at 674 K ranged from 0.005 to 0.008 GPa. The calculation time was 500 ps to ensure that the simulation reaches equilibrium. The results are presented in Figure 6.

Consistent with the reported results, NAP droplets were rapidly disrupted and diffused in SC-cyclohexane.[32] With the increase in the density of cyclohexane, the solubility of SC-cyclohexane to PAHs was decreased gradually. In agreement with the previous sections, the solvent density played a dominant role in the dissolution of NAP droplets and BghiP droplets. In 0.10 g/cm^3 of SC-cyclohexane, the shape of the spherical oil droplets comprising NAP molecules was severely disrupted and NAP molecules could diffuse rapidly and uniformly in SC-cyclohexane. With the increase in the cyclohexane density, NAP molecules started to agglomerate. The phenomenon mentioned above was more obvious for BghiP droplets. BghiP molecules rapidly dissolved in SC-cyclohexane at 0.10 g/cm^3. However, with the rise of the density of cyclohexane, the solubility of BghiP deteriorated, and a T-shaped stacking of BghiP molecules was observed. In SC-cyclohexane at 0.30 g/cm^3, there was a stable agglomerate of BghiP molecules in the solvent box. The agglomerates existed as dimers and trimers, similar to asphaltene $\pi-\pi$ stacking, as shown in Supporting Figure 3. In contrast, the NAP agglomerates formed in SC-cyclohexane were unstable, as the location of the enriched regions varied randomly throughout the simulation.

An independent gradient model based on the Hirshfeld partition (IGMH)analysis was built to explain the type of interaction of its dimer.[33] In the IGMH analysis, the symbol $(\lambda_2)\rho$ is defined to indicate the type, location, and strength of the weak interaction, corresponding to the equivalence surface in Supporting Figure 4(a). ρ denotes the actual electron density of the current system. The large value of ρ can represent a stronger interaction. λ_2 expresses the second largest eigenvalue of the electron density Hessian matrix, and sign() means to take the sign. If λ_2 at a position in the interaction region was less than 0, then there was an attraction between the atoms and vice versa, representing a mutual repulsion. In accordance with Atoms-in-Molecules (AIM) theory, the value of sign (λ_2) at the bond critical point was 1 such that the blue area in Supporting Figure 4(c) represents a strong attractive effect, of which the most common form was hydrogen bonding. Since the sign (λ_2) value in the ring or cage was +1, the red region in Supporting Figure 4(c) indicates the strong steric hindrance of the aromatic ring structure. The green region denotes the van der Waals effect with a small value of ρ and a significant fluctuation in the value of the symbol (λ_2). As depicted in Supporting Figure 4(c), the region was roughly divided into three parts along the x-axis of the symbol $(\lambda_2)\rho$, representing different types of weak interactions. The main interactions were dominated by the van der Waals effect indicated (green) and the strong spatial potential resistance (red), primarily showing peaks in the range of 0.01−0.02. Although there are still strong attractions (blue), the points in this region were sparsely distributed. Accordingly, the interaction between PAHs was mainly van der Waals effect between aromatic cores, and there were continuous, parallel green planes between their dimers, i.e., a typical $\pi-\pi$ stacking feature.

3.2.2. Effect of Temperature. The MD simulation method was used to study the effect of temperature on the dissolution

https://doi.org/10.1021/acsomega.3c04101
ACS Omega 2024, 9, 252−263

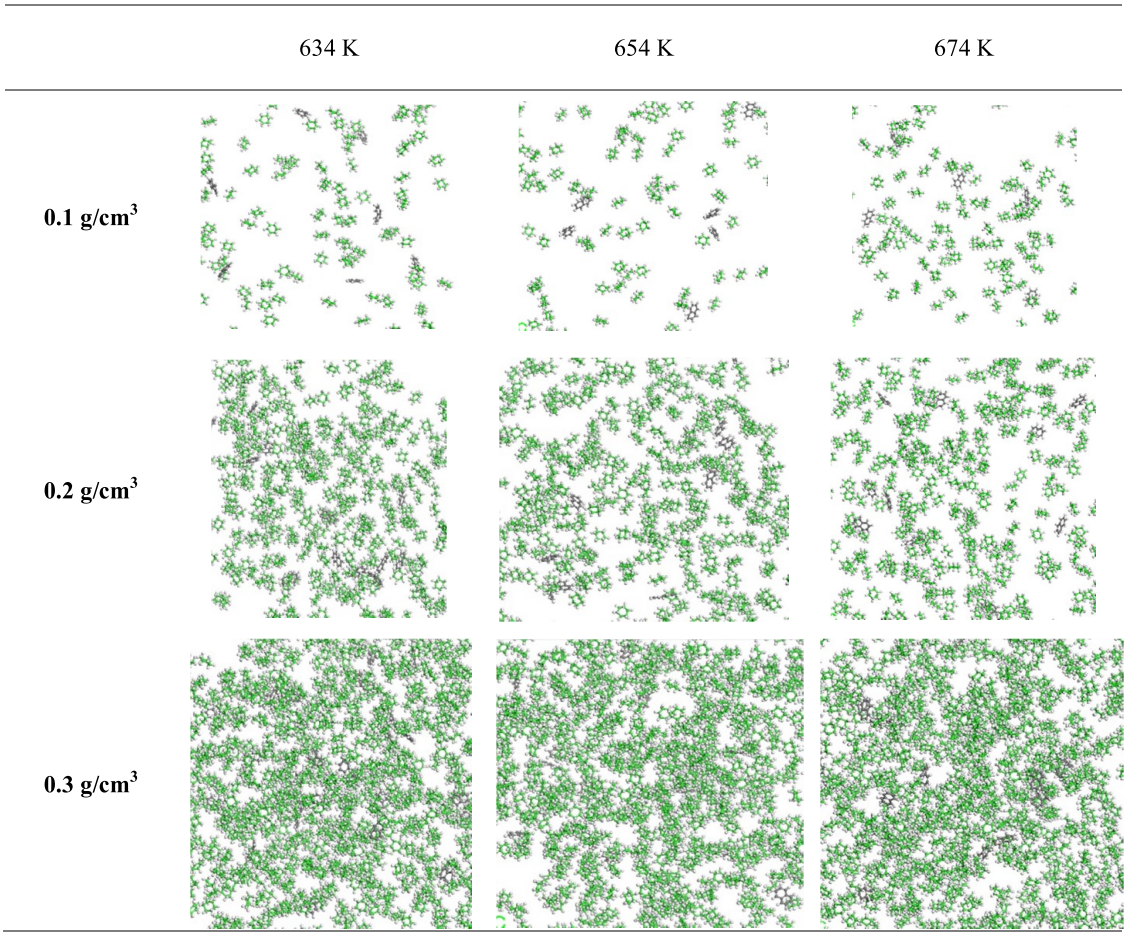

Figure 7. Dissolution of NAP droplets in SC-cyclohexane at different temperatures.

of NAP and BghiP droplets in SC-cyclohexane. The temperature was in the range of 634−674 K, and the density of SC-cyclohexane was 0.10−0.30 g/cm^3. The simulation time is 500 ps. The results are shown in Figures 7 and 10.

Regardless of the change in cyclohexane density, the increase in the temperature slightly promoted the dissolution of the NAP oil droplets. In the low- and medium-temperature regions, the dissolution of BghiP droplets in SC-cyclohexane was similar to that of NAP droplets. However, in the high-temperature regions, the dissolution behavior of NAP molecules and BghiP molecules was significantly different. The NAP molecules still largely dissolved into cyclohexane as monomers. A considerable number of BghiP molecules dissolved in SC-cyclohexane as monomers or dimers. However, most of the BghiP droplets were still agglomerated together, similar to the coking precursors during the pyrolysis of the heavy oil.

As depicted in Figures 7 and 8, the lower cyclohexane density and the appropriate temperature were conducive to increasing the solubility of cyclohexane for NAP droplets and BghiP droplets.

3.2.3. Dissolution of Heavy Oil Consisting of PAH Mixtures in SC-Cyclohexane. The dissolution behaviors of pure NAP oil droplets and BghiP oil droplets in SC-cyclohexane were stated above, whereas heavy oil often comprises aromatics with different polymerization degrees. Thus, the dissolution behaviors of a mixture of PAHs, $BghiP_{80}NAP_{20}$ (the subscript represents the ratio of Benzo-[ghi]perylene and Naphthalene in the oil droplets) were studied through MD simulation.

MD simulations were performed for the dissolution of oil droplets with an initial BghiP fraction of 80 wt % in SC-cyclohexane at three cyclohexane densities (i.e.,0.10, 0.20, and 0.30 g/cm^3) at a fixed temperature of 673 K. Figure 9 presents the dissolution behavior with an increase in the simulation time. The increase in the density of cyclohexane adversely affected the dissolution of the PAH mixture in SC-cyclohexane. At a density of cyclohexane of 0.10 g/cm^3, only PAHs were mainly present as monomers in the solvent box. After the simulation for 125 ps, the mixture placed in the center of the solvent box started to dissolve into cyclohexane. Nevertheless. when the density of cyclohexane was increased to 0.20 or 0.30 g/cm^3, there was still a significant aggregate of the mixture. Both PAH monomers and agglomerates existed in the cyclohexane phase after the simulation for 500 ps. Furthermore, a similar phenomenon was identified in the simulation at low density or high density, and light PAHs preferentially dissolved into the cyclohexane phase.

Compared with pure BghiP and NAP systems, an indistinct difference was identified in the dissolution of the mixture systems as shown in Figure 10. With the increase of temperature, the mixture of oil droplets was more evenly dispersed in the solvent box. After simulation for 500 ps, the oil droplets of $BghiP_{80}NAP_{20}$ were aggregated in the solvent box. At different temperatures, the content of $BghiP_{80}NAP_{20}$ was reduced with the rise of the temperature compared with the

https://doi.org/10.1021/acsomega.3c04101
ACS Omega 2024, 9, 252−263

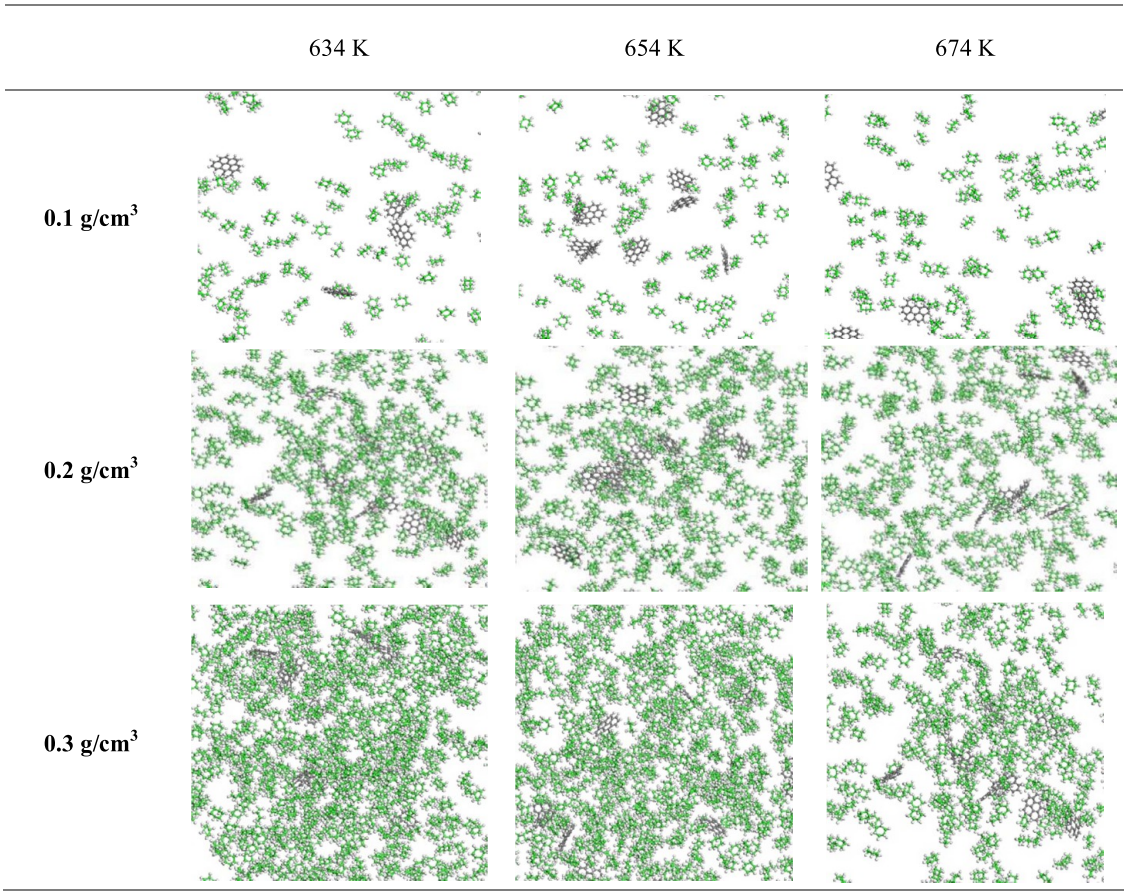

Figure 8. Dissolution of BghiP droplets in SC-cyclohexane at different temperatures.

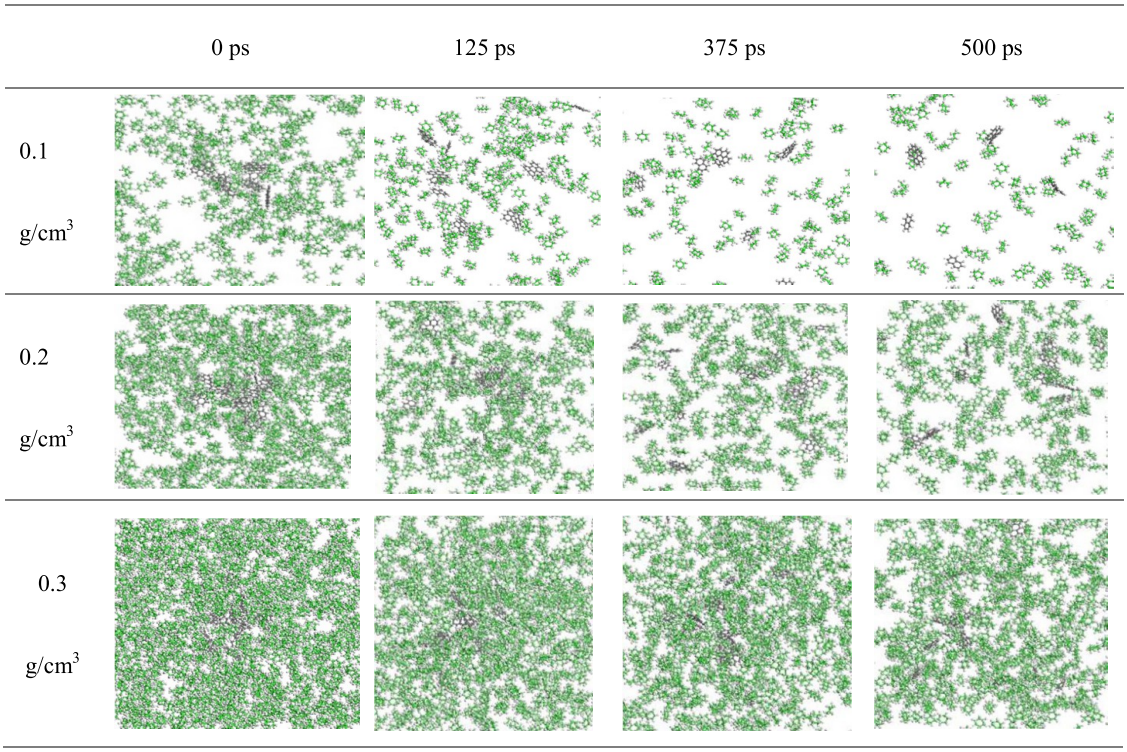

Figure 9. Dissolution procedure of $BghiP_{80}NAP_{20}$ oil droplets in SC-cyclohexane at varied densities at a temperature of 674 K.

content at 0 ps, suggesting that the increase in the temperature can facilitate the dissolution of a polycyclic aromatic hydrocarbon mixture in SC-cyclohexane. Most of the oil droplets of $BghiP_{80}NAP_{20}$ were completely separated, with a

https://doi.org/10.1021/acsomega.3c04101
ACS Omega 2024, 9, 252−263

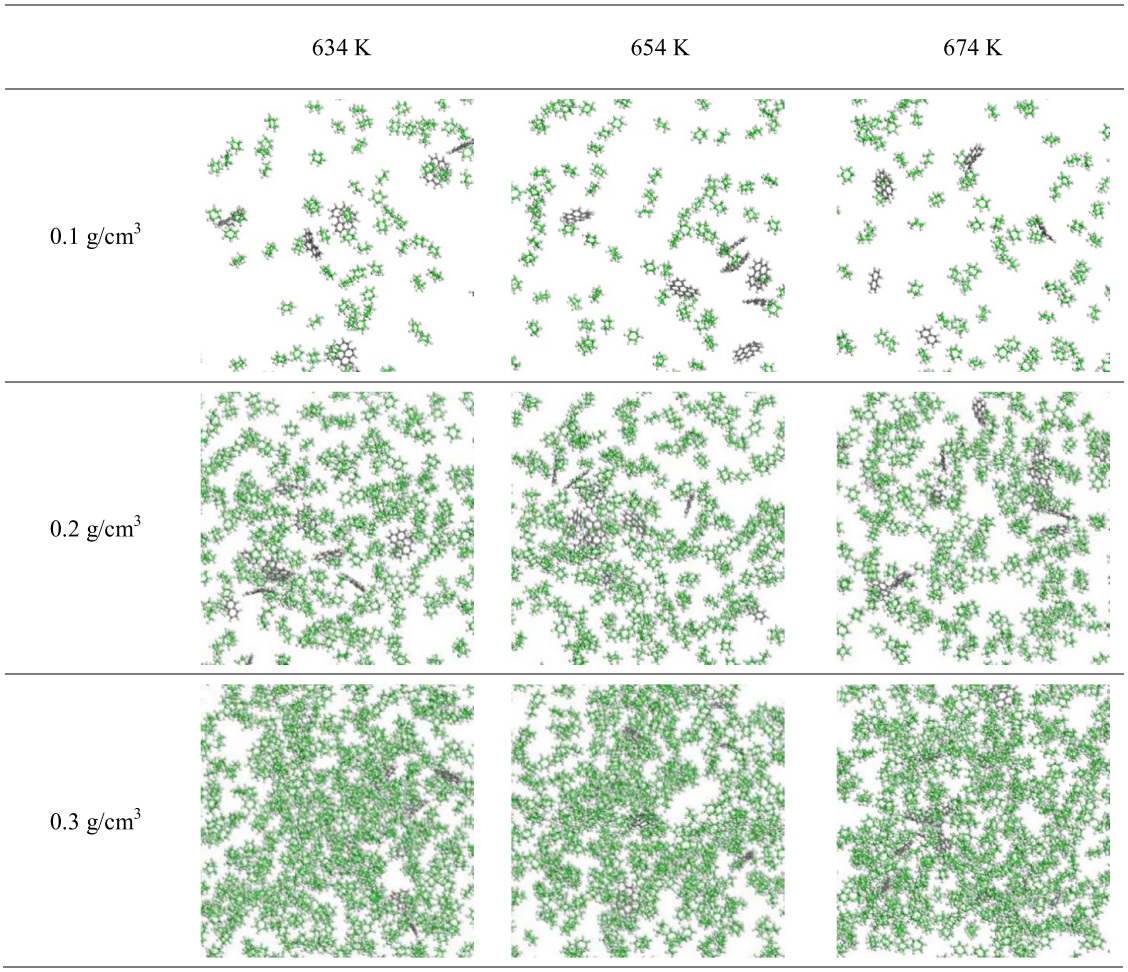

Figure 10. Dissolution of $BghiP_{80}NAP_{20}$ droplets in SC-cyclohexane at different temperatures.

small number of condensations. The initial content of BghiP was significantly reduced such that the dissolution of the polycyclic aromatic hydrocarbon mixture in the cyclohexane phase was expedited, and the oil droplets were completely dissociated. The number of PAH molecules with NAP as the main component in the cyclohexane phase was elevated such that the size of the oil droplets was reduced. NAP diffused in the solvent as a monomer, whereas BghiP existed as a dimer. As indicated by the comparison of the images in Figures 7−9, light PAHs were more soluble than heavy PAHs in SC-cyclohexane.

3.3. Effect of the Dissolution Behavior of PAHs on Pyrolysis of Heavy Oil in SC-Cyclohexane. Based on the literature reported and the MD simulation results of this work, the upgrading of heavy oil in SC-cyclohexane and SCW was compared.

The main difference between the dissolution of PAHs in SC-cyclohexane and SCW is concentrated in the low-density region. In low-density SC-cyclohexane, solvent molecules will form a solvent box around the BghiP to avoid agglomeration between the BghiP. In the presence of the SCW, the solubility of SCW to light PAHs will be limited due to the repulsion between PAHs and SCW.[3]

With the increase in the temperature and density, the solubility of SCW for PAHs was increased and the phase structures of PAHs in SCW and SC-cyclohexane tended to be consistent. In the condensed emulsion obtained in SCF with moderate density and temperature, most of the light PAHs dissolved in the SCF phase, whereas the heavy PAHs were enriched in oil droplets with smaller particle sizes. Motivated by the $\pi-\pi$ interactions, the oil droplets were successively rearranged into a supramolecular structure, similar to the coke structure. Both experiments and kinetic calculations have confirmed that the autocatalysis of coke can facilitate the polymerization of PAHs.[34] Metal heteroatoms can be effectively removed simultaneously by preferentially and rapidly condensing heavy PAHs enriched with oil droplets into coke.

Under the SCF with high densities and high temperatures, a pseudo-homogeneous phase was created, where light and heavy oil components simultaneously dissolved into a continuous SCF phase. The cracking of PAH alkyl substituents and the condensation of PAHs has been confirmed as the main process of heavy oil pyrolysis.[35] The cracking process of alkyl substituents is initiated by the homolytic cleavage between α and β carbon atoms; subsequently, the aliphatic carbon radicals generated by other alkyl substituents are subjected to bimolecular H-abstraction to propagate the cracking process.[36] The heavy oil fractions are upgraded to a light oil fraction. In SCF, the recombination of alkyl radicals generated by cleavage of aliphatic substituents with an activation energy of 317 kJ/mol is partially inhibited such that the initial efficiency of the cracking reaction can be ensured.[37] Besides, the apparent reaction rate is dominated by the diffusion rate of the reactants

https://doi.org/10.1021/acsomega.3c04101
ACS Omega 2024, 9, 252−263

when the activation energy of the bimolecular H-abstraction only reached 40 kJ/mol.[38] At this time, the greater diffusion rate in the SC-cyclohexane phase should be more conducive to the progress of H-abstraction than in the SCW phase. At the reaction temperatures employed in this study, the aggregation reaction of PAHs was a secondary reaction of the cleavage of the aliphatic substituents of PAHs.[39−43] From the perspective of reaction kinetics, condensation can be effectively suppressed by strengthening the interaction between cracking and the interaction of SC-cyclohexane and heavy PAHs.[44] Accordingly, when upgrading viscosity reduction is required, a low-density and high-temperature zone that is capable of accelerating cracking but inhibiting condensation should be selected.

4. CONCLUSIONS

In this study, the dissolution behavior of PAHs in SC-cyclohexane was investigated through MD simulation, which can be conducive to providing insights into the effect of dissolution behavior on the pyrolysis of heavy oil in SC-cyclohexane. As indicated by the results, the density of SC-cyclohexane played a dominant role in the dissolution of PAHs. At low densities, cyclohexane molecules formed solvent shells around PAH molecules, reduced the concentration of PAHs in local areas, and inhibited the coke formation of PAHs. The intermolecular interaction of PAHs was promoted with an increase in the density. The interaction between PAHs and cyclohexane was reduced with an increase in the density. Compared with NAP (light PAHs) with two aromatic rings, the solubility of BghiP (heavy PAHs) with six aromatic rings in SC-cyclohexane was more affected by temperature since the increase of the temperature exerted a stronger promoting effect on $\pi-\pi$ stacking between heavy PAHs. The light PAHs preferentially dissolved into the cyclohexane phase, while the heavy PAHs were concentrated in the reduced oil droplets during the dissolution of the oil droplets comprising PAH mixtures. Thus, a decrease of the cyclohexane density and the appropriate temperature can expedite the dissolution and pyrolysis of heavy oil in SC-cyclohexane.

■ ASSOCIATED CONTENT

Data Availability Statement

The data that support the findings of this study are available from the corresponding author upon reasonable request.

Supporting Information

The Supporting Information is available free of charge at https://pubs.acs.org/doi/10.1021/acsomega.3c04101.

Molecular structures of different NAP and BghiP; schematic diagram of SC-cyclohexane cube box; configurations of a dimer of BghiP formed in SC-cyclohexane; and model properties of PAHs (PDF)

■ AUTHOR INFORMATION

Corresponding Author

Ting Yan − *Shaanxi Key Laboratory of Chemical Reaction Engineering, School of Chemistry and Chemical Engineering, Yan'an University, Yan'an 716000 Shaanxi, China;* orcid.org/0000-0001-8966-1902; Email: 9992777@163.com

Authors

Xiangbo Zhao − *Shaanxi Key Laboratory of Chemical Reaction Engineering, School of Chemistry and Chemical Engineering, Yan'an University, Yan'an 716000 Shaanxi, China; Shaanxi Gold Group Xi'an Qinjin Co., Ltd., Xi'an 710300 Shaanxi, China*

Litao Wang − *Project Office of Heavy to Light Conversion, Petrochemical Research Institute, Beijing 100007, China*

Shuai Liu − *Shaanxi Key Laboratory of Chemical Reaction Engineering, School of Chemistry and Chemical Engineering, Yan'an University, Yan'an 716000 Shaanxi, China*

Xuan Luo − *Shaanxi Key Laboratory of Chemical Reaction Engineering, School of Chemistry and Chemical Engineering, Yan'an University, Yan'an 716000 Shaanxi, China*

Mengran Zhang − *Shaanxi Key Laboratory of Chemical Reaction Engineering, School of Chemistry and Chemical Engineering, Yan'an University, Yan'an 716000 Shaanxi, China*

Feng Fu − *Shaanxi Key Laboratory of Chemical Reaction Engineering, School of Chemistry and Chemical Engineering, Yan'an University, Yan'an 716000 Shaanxi, China;* orcid.org/0000-0002-3778-1344

Xiaoming Gao − *Shaanxi Key Laboratory of Chemical Reaction Engineering, School of Chemistry and Chemical Engineering, Yan'an University, Yan'an 716000 Shaanxi, China*

Complete contact information is available at: https://pubs.acs.org/10.1021/acsomega.3c04101

Notes

The authors declare no competing financial interest.

■ ACKNOWLEDGMENTS

The authors gratefully appreciate the following financial supports: the Major Research and Development Project of Central Government Guides Local Science and Technology Development Professional Technology Innovation Platform (no. 2019ZY-CXPT-08), the National Natural Science Foundation of China (nos. 22068037 and 21908187), Natural Science Basic Research Program of Shaanxi Province (no. 2021JQ-615), Ph.D. research startup foundation of Yan'an University (YDBK2019-04), Yan'an High-level Talents Special Foundation (no. 2019-14), Youths Talents Support Program of Shaanxi Association for Science and Technology (no. 20200607), Yan'an Science and Technology Bureau (no. 2019ZCGY-002), and Yan'an University Industry-University-Research Cooperation Cultivation Project (no. 2020-10).

■ REFERENCES

(1) Aleklett, K.; Höök, M.; Jakobsson, K.; Lardelli, M.; Snowden, S.; Söderbergh, B. The Peak of the Oil Age: Declining world oil production will halt economic growth - Sydney Ideas - The University of Sydney. *Energy Policy* **2010**, *38*, 1398−1414.

(2) Hosseinpour, M.; Fatemi, S.; Ahmadi, S. J.; Morimoto, M.; Akizuki, M.; Oshima, Y.; Fumoto, E. The synergistic effect between supercritical water and redox properties of iron oxide nanoparticles during in-situ catalytic upgrading of heavy oil with formic acid. Isotopic study. *Appl. Catal., B* **2018**, *230*, 91−101.

(3) Qu, H.; Gong, J. H.; Tan, X. C.; Yuan, P. Q.; Yuan, W. K. Dissolution of polycyclic aromatic hydrocarbons in subcritical and supercritical water: a molecular dynamics simulation study. *Chem. Eng. Sci.* **2018**, *195*, 958−967.

(4) Ancheyta, J. Modelling of processes and reactors for upgrading of heavy petroleum. *Focus Catal.* **2013**, *2013* (11), No. 8.

(5) Bello, S. S.; Wang, C.; Zhang, M.; Gao, H.; Han, Z.; Shi, L.; Su, F.; Xu, G. A Review on the reaction mechanism of hydro-

desulfurization and hydrodenitrogenation in heavy oil upgrading. *Energy Fuels* **2021**, *35*, 10998−11016.
(6) Hosseinpour, M.; Fatemi, S.; Ahmadi, S. J. Catalytic cracking of petroleum vacuum residue in supercritical water media: Impact of α-Fe2O3 in the form of free nanoparticles and silica-supported granules. *Fuel* **2015**, *159*, 538−549.
(7) Jedlovszky, P.; Vincze, A.; Horvai, G. Full description of the orientational statistics of molecules near to interfaces. Water at the interface with CCl4. *Phys. Chem. Chem. Phys.* **2004**, *6*, 1874−1879.
(8) Lümmen, N. ReaxFF-molecular dynamics simulations of non-oxidative and non-catalyzed thermal decomposition of methane at high temperatures. *Phys. Chem. Chem. Phys.* **2010**, *12*, 7883−7893.
(9) Agrawalla, S.; Duin, A. Development and Application of a ReaxFF reactive force field for hydrogen combustion. *J. Phys. Chem. A* **2011**, *115*, 960−972.
(10) Han, Y.; Jiang, D.; Zhang, J.; Li, W.; Gan, Z.; Gu, J. Development, applications and challenges of ReaxFF reactive force field in molecular simulations. *Front. Chem. Sci. Eng.* **2016**, *10*, 16−38.
(11) Zhang, Y.-M.; Li, J.; Wang, J.; Yang, X.; Wang, B. ReaxFF MDSs-based studies on gasification of glucose in supercritical water under microwave heating. *Int. J. Hydrogen Energy* **2016**, *41*, 13390−13398.
(12) Akiya, N.; Savage, P. E. Roles of water for chemical reactions in high-temperature water. *Chem. Rev.* **2002**, *102* (8), 2725−2750.
(13) Bai, B.; Liu, Y.; Meng, X.; Liu, C.; Zhang, H.; Zhang, W.; Jin, H. Experimental investigation on gasification characteristics of polycarbonate (PC) microplastics in supercritical water. *J. Energy Inst.* **2020**, *93*, 624−633.
(14) Chen, J.; Fan, Y.; Zhao, X.; E, J.; Xu, W.; Zhang, F.; Liao, G.; Leng, E.; Liu, S. Experimental investigation on gasification characteristic of food waste using supercritical water for combustible gas production: Exploring the way to complete gasification. *Fuel* **2020**, *263*, No. 116735.
(15) Kayode, I.; Hassanzadeh, M. Z. Phase equilibria of water-hydrocarbon (pentane to heavy oils) systems in the near-critical and supercritical water regions - A literature review. *J. Supercrit. Fluids* **2021**, *178*, No. 105356.
(16) Watanabe, M.; Kato, S. N.; Ishizeki, S.; Inomata, H.; Smith, R. L. Heavy oil upgrading in the presence of high density water: Basic study. *J. Supercrit. Fluids* **2010**, *53*, 48−52.
(17) Morimoto, M.; Sugimoto, Y.; Saotome, Y.; Sato, S.; Takanohashi, T. Effect of supercritical water on upgrading reaction of oil sand bitumen. *J. Supercrit. Fluids* **2010**, *55*, 223−231.
(18) Cheng, Z.-M.; Ding, Y.; Zhao, L.; Yuan, P.; Lu, S.; Yuan, W. Effects of supercritical water in Vacuum residue upgrading. *Energy Fuels* **2009**, *23*, 178−183.
(19) Sulaimon, A. A.; Falade, G. K. New two-phase and three-phase thermodynamic models for predicting wax precipitation in hydrocarbon mixtures. *J. Petrol. Sci. Eng.* **2022**, *208*, No. 109707.
(20) Zheng, M.; Li, X.; Liu, J.; Guo, L. Initial Chemical Reaction Simulation of Coal Pyrolysis via ReaxFF Molecular Dynamics. *Energy Fuels* **2013**, *27*, 2942−2951.
(21) Zheng, M.; Li, X.; Liu, J.; Wang, Z.; Gong, X.; Guo, L.; Song, W. Pyrolysis of Liulin coal simulated by GPU-Based ReaxFF MD with cheminformatics analysis. *Energy Fuels* **2014**, *28*, 522−534.
(22) Zhou, J.; Lu, X.; Wang, Y.; Shi, J. Molecular dynamics simulation of supercritical water. *Acta Phys. Chim. Sin.* **1999**, *15*, 1017−1022.
(23) Xin, S.-M.; Liu, Q.; Wang, K.; Chen, W.; Yuan, P.; Chen, Z.; Yuan, W. Solvation of Asphaltenes in Supercritical Water: A Molecular Dynamics Study. *Chem. Eng. Sci.* **2016**, *146*, 115−125.
(24) Liu, X.-Q.; Qu, H.; Yang, J.; Yuan, P.; Yuan, W. Visbreaking of heavy oil in supercritical benzene. *Energy Fuels* **2019**, *33*, 1074−1082.
(25) Ding, L.; Wang, L.; Yang, J.; Yuan, P.; Huang, Z. The visbreaking of heavy oil in supercritical cyclohexane: the effect of H-donation. *Processes* **2022**, *10*, No. 914.
(26) Carr, A. G.; Class, C. A.; Lai, L.; Kida, Y.; Monrose, T.; Green, W. H. Supercritical water treatment of crude oil and hexylbenzene: an experimental and mechanistic study on alkylbenzene decomposition. *Energy Fuels* **2015**, *29*, 5290−5302.
(27) Kirkwood, J. G. Statistical mechanics of fluid mixtures. *J. Chem. Phys.* **1935**, *3*, 300−313.
(28) Headen, T. F.; Boek, E. S.; Jackson, G.; Totton, T. S.; Müller, E. A. Simulation of asphaltene aggregation through molecular dynamics: Insights and Limitations. *Energy Fuels* **2017**, *31*, 1108−1125.
(29) Fujisawa, T.; Terazima, M.; Kimura, Y.; Maroncelli, M. Resonance Raman study of the solvation of p -nitroaniline in supercritical water. *Chem. Phys. Lett.* **2006**, *430*, 303−308.
(30) Oka, H.; Kajimoto, O. UV absorption solvatochromic shift of 4-nitroaniline in supercritical water. *Phys. Chem. Chem. Phys.* **2003**, *5*, 2535−2540.
(31) Manna, B.; Datta, S.; Ghosh, A. Understanding the dissolution of softwood lignin in ionic liquid and water mixed solvents. *Int. J. Biol. Macromol.* **2021**, *182* (82), 402−412.
(32) Zhu, C.-C.; Ren, C.; Tan, X.; Chen, G.; Yuan, P.; Cheng, Z.; Yuan, W. Initiated pyrolysis of heavy oil in the presence of near-critical water. *Fuel Process. Technol.* **2013**, *111*, 111−117.
(33) Lu, T.; Chen, Q. Independent gradient model based on Hirshfeld partition: A new method for visual study of interactions in chemical systems. *J. Comput. Chem.* **2022**, *43*, 539−555.
(34) Liu, Q.-K.; Xu, Y.; Tan, X.; Yuan, P.; Cheng, Z.; Yuan, W. Pyrolysis of Asphaltenes in Subcritical and Supercritical Water: Influence of H-Donation from Hydrocarbon Surroundings. *Energy Fuels* **2017**, *31*, 3620−3628.
(35) Kozhevnikov, I. V.; Nuzhdin, A. L.; Martyanov, O. N. Transformation of petroleum asphaltenes in supercritical water. *J. Supercrit. Fluids* **2010**, *55*, 217−222.
(36) Li, N.; Zhang, X.; Zhang, Q.; Chen, L.; Ma, L.; Xiao, X. Reactivity and structural changes of asphaltene during the supercritical water upgrading process. *Fuel* **2020**, *278*, No. 118331.
(37) Savage, P. E. Mechanisms and kinetics models for hydrocarbon pyrolysis″. *J. Anal. Appl. Pyrol.* **2000**, *54*, 109−126.
(38) Watanabe, M.; Tsukagoshi, M.; Hirakoso, H.; Adschiri, T.; Arail, K. Kinetics and product distribution of n-hexadecane pyrolysis. *AIChE J.* **2000**, *46*, 843−856.
(39) Leininger, J. P.; Minot, C.; Lorant, F.; Behar, F. Density functional theory investigation of competitive Free-Radical processes during the thermal cracking of methylated polyaromatics: estimation of kinetic parameters. *J. Phys. Chem. A* **2007**, *111*, 3082−3090.
(40) Hemelsoet, K.; Moran, D.; Speybroeck, V. V.; Waroquier, M.; Radom, L. An assessment of theoretical procedures for predicting the thermochemistry and kinetics of hydrogen abstraction by methyl radical from benzene. *J. Phys. Chem. A* **2006**, *110*, 8942−8951.
(41) Sabbe, M. K.; Vandeputte, A. G.; Reyniers, M. F.; Speybroeck, V. V.; Waroquier, M.; Marin, G. B. Ab initio thermochemistry and kinetics for carbon-centered radical addition and β-Scission reactions. *J. Phys. Chem. A* **2007**, *111*, 8416−8428.
(42) Speybroeck, V. V.; Neck, D. V.; Waroquier, M.; Wauters, S.; Saeys, M.; Marin, G. B. Ab initio study of radical addition reactions: addition of a primary ethylbenzene radical to ethene. *J. Phys. Chem. A* **2000**, *104* (46), 10939−10950.
(43) Van Speybroeck, V.; Hemelsoet, K.; Waroquier, M.; Marin, G. Reactivity and aromaticity of polyaromatics in radical cyclization reactions. *Int. J. Quantum Chem.* **2004**, *96*, 568−576.
(44) Liu, J.; Xing, Y.; Chen, Y.; Yuan, P.; Cheng, Z.; Yuan, W. Visbreaking of heavy oil under supercritical water environment. *Ind. Eng. Chem. Res.* **2018**, *57*, 867−875.

https://doi.org/10.1021/acsomega.3c04101
ACS Omega 2024, 9, 252−263